Simulated changes due to global warming in daily precipitation means and extremes and their interpretation using the gamma distribution

I. G. Watterson and M. R. Dix

Division of Atmospheric Research, Commonwealth Scientific and Industrial Research Organisation, Aspendale, Victoria, Australia

Received 10 September 2002; revised 24 February 2003; accepted 19 March 2003; published 5 July 2003.

[1] The potential change in precipitation due to global warming is studied using five-member ensembles of climate simulations by the CSIRO Mark 2 atmosphere-ocean model for the period 1871–1990 and forward to 2100 under both the Special Report on Emission Scenarios (SRES) A2 (rapid CO_2 increase) and B2 (moderate increase) forcing scenarios. The mean surface warming for the period 1961–1990 is 0.3 K. The warming from 1961–1990 to 2071–2100 is 3.5 K under A2, 29% more than for B2, and with a very similar spatial pattern. The daily precipitation (P) frequency distributions for January and July days in these periods are presented, focusing on the A2 case. The distributions for wet days at each point are approximated by the gamma distribution. The global mean P increase of around 6%, in both months, is related to a mean increase in the gamma's scale parameter of 18%, offset by small decreases in the shape parameter and wet day frequency. However, local changes of opposite signs also occur, especially in the tropics. Ensemble averages of 30-year extreme daily precipitation for January and July, and other months, are generally greater for 2071–2100 than for 1961–1990, with an average increase of 14%. Extreme value theory based on the monthly gamma distributions provides a good match to these values. The theory is extended to the annual case. In general, the 1961–1990 extremes peak in the subtropical rainbands in the model, where increases of 10 to 30% are common. Larger relative increases occur in polar regions, and also over northern land in January. *INDEX TERMS:* 1610 Global Change: Atmosphere (0315, 0325); 1655 Global Change: Water cycles (1836); 1869 Hydrology: Stochastic processes; 3337 Meteorology and Atmospheric Dynamics: Numerical modeling and data assimilation; 3354 Meteorology and Atmospheric Dynamics: Precipitation (1854); *KEYWORDS:* daily precipitation, gamma distribution, climate change, extreme rainfall

Citation: Watterson, I. G., and M. R. Dix, Simulated changes due to global warming in daily precipitation means and extremes and their interpretation using the gamma distribution, *J. Geophys. Res.*, *108*(D13), 4379, doi:10.1029/2002JD002928, 2003.

1. Introduction

[2] Recent "transient" climate simulations by coupled atmosphere-ocean global climate models (GCMs) have indicated that the inclusion of the radiative effect of anthropogenic sulfate aerosol improves the realism of the simulation of the past century [*Cubasch et al.*, 2001], particularly for models, including the Commonwealth Scientific and Industrial Research Organisation (CSIRO) Mark 2 GCM [*Gordon and O'Farrell*, 1997; *Hirst*, 1999], that otherwise appear to be too sensitive to the observed greenhouse gas increases. New simulations (or runs) of Mark 2 including sulfate aerosol, representing forcing over 1871–1990, and on to 2100 under both the Special Report on Emission Scenarios (SRES) A2 and B2 scenarios [*Cubasch et al.*, 2001], are presented here.

0148-0227/03/2002JD002928

[3] Five-member ensembles of simulations for both scenarios are used to allow the forced response of the model climate system to be more accurately determined, above internally generated variability. This is particularly important for the assessment of daily precipitation, P, which is the focus of the study. Studies based on earlier CSIRO models [*Gordon et al.*, 1992; *Hennessy et al.*, 1997], and several other GCMs, found that global warming often led to decreases in the frequency of "wet" days, but also increases in the frequency of intense daily precipitation events, particularly in the subtropics. Recently, *Semenov and Bengtsson* [2002] analyzed the distribution of wet day amounts at each grid square over the globe in a transient climate simulation and approximated each by a gamma distribution, with varying "scale" and "shape" parameters (see Appendix B that follows for the definitions). Over the period of the simulation, increases in the scale parameter occurred over much of the land, consistent with observed trends determined for certain regions by *Groisman et al.*

[1999], but decreases occurred over subtropical oceans. Comparable results from two other GCMs have also been reported by *Wilby and Wigley* [2002].

[4] *Katz* [1999] showed that extreme (maximum) values from a gamma distribution are sensitive to the scale parameter, and indeed, *Kharin and Zwiers* [2000] found widespread increases of extreme precipitation in a transient simulation. The trends from these studies vary considerably, however, particularly in the tropics, and an assessment of the distributions and extremes in the Mark 2 ensembles is clearly warranted. The extent to which extremes of the simulated precipitation can be related to the gamma distribution using extreme value theory, as proposed by *Katz* [1999], will also be assessed.

[5] The applicability of the gamma distribution and of extreme value theory to simulated precipitation would aid the assessment of the impacts of climate change [e.g., *Mearns et al.*, 1997], particularly with regard to return periods of intense events, which can not be determined from short transient runs. However, it has long been recognized that GCM's produce smaller extremes than those in observational station data. Mark 2 includes a relatively accurate semi-Lagrangian transport scheme for water vapor, and precipitation is generated through both saturation and parameterized Arakawa convection scheme including a mass flux [*Watterson*, 1998]. However, the GCM can only represent averages of moisture quantities within its nine (sigma coordinate) vertical layers and over grid squares of some 3.2° latitude and 5.6° longitude. *Konrad* [2001] shows that observed extreme precipitation events over the United States rapidly decrease in intensity as station data are (in effect) averaged over increasingly large regions. They remain larger than values simulated by Mark 2, as we shall see, although being two-day means evaluated over circular regions with arbitrary centers the comparison is somewhat unfair. Indeed, *Osborn and Hulme* [1998] found that simple station averaging is likely to overestimate the variability of daily grid square means, particularly for small station densities. They demonstrated reasonable agreement between standard deviations of daily precipitation from various GCMs and observations over Europe in an analysis that compensates for this effect. While the Mark 2 GCM climate change results will require further interpretation, and "downscaling" with regard to the impacts of local extreme precipitation, we may anticipate that they have relevance to regional impacts. Given the statistical focus of the present study, it is worth noting that a more physical interpretation of mean precipitation changes in Mark 2 is offered by *Watterson* [1998].

[6] In the following section the transient climate simulations for two scenarios of net greenhouse gas (GHG) in the 21st century are presented, with the details reserved for Appendix A. The climatic change is briefly compared with previous work. In section 3, the precipitation characteristics for the periods 1961–1990 and 2071–2100 of the larger (A2) forcing scenario, focusing on January and July days, are presented. The gamma distributions that approximate the precipitation frequencies are presented. A brief interpretation of changes in the mean precipitation based on the gamma parameters is offered. We turn to the extremes of daily precipitation, initially from the thirty January and July months of each case, in section 4. The degree that the extreme value theory, based on the gamma fits, can match the simulated extremes and their changes is considered. Both simulated and theoretical 30-year extremes (the annual case) are then presented. A discussion focusing on the tropical results and the conclusions follow.

2. Transient Climate Simulations

2.1. Ensembles

[7] Five simulations of the period 1871–1990 were performed by the Mark 2 GCM. These were initialized at 50-year intervals of a control simulation, as detailed in Appendix A. The runs incorporated the radiative effects of changing CO_2, other greenhouse gases, and ozone, as well as the direct effect of atmospheric sulfate over the period. The five simulations were each continued to 2100 with the SRES B2 forcing scenario (prior to 1990 the name B2 is used here only for convenience). The first simulation was also continued to 2100 with the A2 forcing scenario. These initial simulations are those reported by *Cubasch et al.* [2001]. A further four A2 simulations for the period 1991–2100 are also available, with varying initializations based on the first 1871–1990 run (see Appendix A).

[8] The time series of ensemble means (each averages of five series) of the global and annual mean surface temperature T are shown in Figure 1. Even without temporal smoothing, both series show rather steady warming. In addition, there is no broadening over time of the spread of the global and annual mean T across the five B2 simulations, as evidenced by the maxima and minima series also shown in Figure 1. As there is no discernable drift in the climate of the control run, we can take the trends in the B2 ensemble mean to be the response of the model to the applied atmospheric forcing over the full period, subject to the retarding effect of oceanic heat uptake [e.g., *Watterson*, 2000]. Further, the initial run for 1871–1990 is typical of the others, so that the A2 ensemble initialized from that run can reasonably be compared with the other ensemble over those earlier years and the later years (see Appendix A for a fuller discussion).

[9] The mean warming from 1881 to 2000, using 21-yr running means, in the (B2) ensemble is 0.78 K. Comparison with the earlier simulation with CO_2 forcing alone [*Hirst*, 1999] indicates that the addition of sulfate and ozone changes reduces the warming by 0.36 K. Averaged over 1961–1990 the reduction is 0.18 K. The additional forcing evidently improves the agreement of the model with the observed change described by *Folland et al.* [2001]. There is a clear difference between the A2 and B2 temperatures over the period 2010–2100 due to the differing forcings. For several decades the A2 warming is less than the B2 warming, a result typical of simulations reported by *Cubasch et al.* [2001]. This is due to the much larger anthropogenic sulfate loading in A2 during 2020 to 2050 when it almost doubles the near-constant B2 value. The loading in A2 exceeds that in B2 by only 20% during 2071–2100. The greater equivalent CO_2 in A2, reaching 4.2 times the 1870 value at 2100 compared with 2.7 times in B2, results in greater mean warming after 2060. The final warmings in each case are among the largest of the nine GCM results reported by *Cubasch et al.* [2001]. The final warming in A2 is also similar to that of the ensemble from the CGCM2 model of *Boer et al.* [2000], analyzed by *Kharin and Zwiers* [2000],

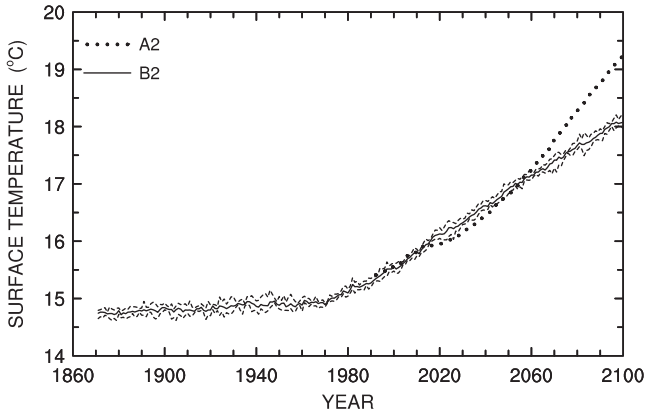

Figure 1. Global and annual mean of surface temperature simulated by the CSIRO GCM in two ensembles. "A2" denotes the mean of five simulations with the A2 forcing scenario, initialized at year 1991. "B2" denotes the mean of five runs of the period 1871–2100, with the B2 scenario from 1991. Also shown (dashed lines) are the series of maximum and minimum values of the five B2 results at each year.

for a 1% compounding GHG scenario, including aerosols, that is similar to A2. The simulation of the ECHAM4/OPYC3 GCM for a GHG scenario intermediate between A2 and B2, which was analyzed by *Semenov and Bengtsson* [2002], produced a warming also intermediate to the Mark 2 results [*Roeckner et al.*, 1999].

[10] Though the series of global mean precipitation rate P from each of the Mark 2 simulations is relatively noisier than for T, there is again a clear difference between the scenarios in the ensemble mean series, as evidenced by Figure 2. The enhanced sulfate in A2 leads to a slight decrease in P around 2020, but otherwise both scenarios produce increasing mean P. Again, the changes are among the larger values reported by *Cubasch et al.* [2001]. Global mean changes are also larger than those of both *Boer et al.* [2000] and *Semenov and Bengtsson* [2002].

2.2. Climatic Changes

[11] Following *Cubasch et al.* [2001], we define climates using a 30-year statistical period and consider the periods at the ends of the full span, namely 1871–1900 and 2071–2100, as well as 1961–1990 and 2021–2050. Averages over the five simulations are used, in each case. The 1961–1990 climate is similar to that from the $1 \times CO_2$ climate of the Mark 2 model with a mixed layer ocean [*Watterson*, 1998], so only a limited consideration of it is needed here. Global mean temperatures and precipitation relative to the simulated 1961–1990 values (the difference denoted by Δ) are given in Table 1. The changes from the earlier period are small, while the 2021–2050 changes are greater in B2. By the final period, the A2 to B2 ratio is larger for ΔT (1.29) than for ΔP (1.20). Both ratios are similar to the mean results from *Cubasch et al.* [2001]. The percentage change in another key moisture quantity, the total water column (or precipitable water) W in Table 1, is much larger than for P, with the ratio (1.33) closer to that of ΔT. This is consistent with the generally small change in relative humidity, given the relatively small warming (hence only weak nonlinearity between changes in absolute humidity and T).

[12] The similarity in ratio between A2 and B2 changes in the final period for W and T holds for both January and July means and at each latitude also, as can be seen from the zonal means for ΔW in Figure 3. The absolute change in W is largest in the tropics, and in the (midlatitude to high latitude) summer due to the greater initial W there. Correlation coefficients between the A2 and B2 spatial fields are around 0.99, for both quantities and both months. Those for precipitation are also high, 0.96 for January and 0.90 for July. There is very little difference between average land or ocean values of the ratio of the A2 to B2 changes in all three quantities. For brevity, we will henceforth consider only the final period of the A2 ensemble, and its comparison with the simulated 1961–1990 period. This focuses on the changes due to CO_2 rather than sulfate.

[13] Zonal means for the January and July mean daily precipitation in 1961–1990 are shown in Figure 4, together with those for 2071–2100. The largest increases are near the equator, and the only zonal mean decreases are in the subtropics. While there is an increase in the water content of the atmosphere (W) everywhere, this does not carry over to P itself. The local percentage changes in P for these months are depicted in Figures 5a and 5b. The values shaded (of magnitude greater than 10%) are mostly statistically significant at the 95% level, at least, based on a standard t-test concerning variation between the ensemble members. Decreases are prevalent in the subtropics and the northern midlatitude land in summer. Sizable increases occur over some land, particularly in winter. Much of this pattern of

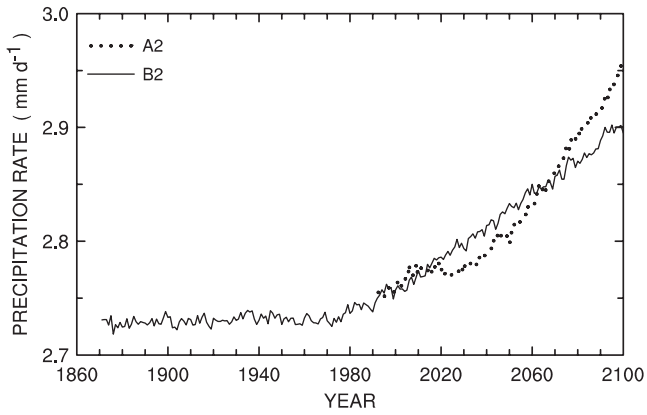

Figure 2. As for Figure 1, but for precipitation rate.

Table 1. Global and Annual Mean Simulated Differences Relative to 1961–1990 for Three 30-Year Periods, Under Two Scenarios for GHG Changes[a]

	ΔT, K		ΔP, %		ΔW, %	
Period	A2	B2	A2	B2	A2	B2
1871–1900		−0.30		−0.26		−2.15
2021–2050	1.28	1.43	1.83	2.58	8.76	9.86
2071–2100	3.49	2.71	6.31	5.27	25.72	19.38

[a]"A2" denotes the mean of five runs with the A2 forcing scenario, initialized at year 1991. "B2" denotes the mean of five simulations of the period 1871–2100, with the B2 scenario from 1991. ΔT is the change in surface temperature (relative to 288.2 K). ΔP is the percentage change in precipitation rate (relative to 2.74 mm d^{-1}). ΔW is the percentage change in the atmospheric water column (relative to 23.8 mm of condensed water).

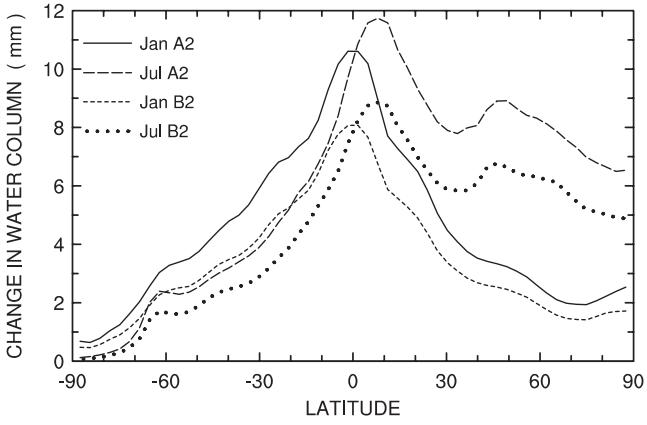

Figure 3. Zonal mean of the change in water column simulated by the CSIRO GCM in January (Jan) and July (Jul). Values for both the A2 and B2 scenarios are shown, and both are changes from 1961–1990 to 2071–2100.

change is seen in seasonal results of *Boer et al.* [2000] and *Semenov and Bengtsson* [2002], although there are also differences. *Semenov and Bengtsson* [2002] find more extensive decreases in the western Pacific Ocean in June–August, and in the Southern Ocean in December–February, for instance. The pattern of annual mean changes from Mark 2, shown in Figure 5c, has much in common with the average over nine GCMs shown by *Cubasch et al.* [2001], an exception being no sub-Saharan increase in Mark 2. Overall means of P and its change in both months are given in Table 2.

3. Distribution of Daily Precipitation

3.1. Simulated Precipitation for 1961–1990 and 2071–2100

[14] Just as there is a clear annual cycle in the mean precipitation, we anticipate a cycle in the frequency distribution of daily precipitation amounts. With the size of the data set provided by the ensembles, we can assess distributions partitioned by the month of the year with some certainty. We focus again on the January and July months, for each of which there is an ensemble total of 4650 days for each 30-year period. Given a trend in mean P the distributions cannot be strictly stationary within such a period. However, any effect of this should be small relative to the differences between the two periods examined here. In any case, it is appropriate to match the period length with that of the extreme value analysis that follows.

[15] We define, first, the frequency, π, of wet days, on which P is greater than a threshold value. The daily rain (including the simulated frozen precipitation) data set was archived using a packed form allowing increments of 0.0023 mm. The smallest archived value is 0.0005 mm, but this represents all actual amounts (including zero) less than or equal to 0.0017 mm. The latter value is much less than is normally measurable at an observational station (typically 0.1 mm [*Groisman et al.*, 1999]), but may conceivably relate well to measurable rain somewhere within a grid square area. In any case, using such a small value as the threshold for defining a wet day is consistent with the gamma distribution theory that follows. Using 0.0017 mm as the threshold, we determine at each grid square a fraction of wet days for each month, averaging over the five simulations. The global map of π values in January is shown in Figure 6. There are locations in both January and July with $\pi = 0$ over actual deserts, while rain falls every day at some tropical grid squares. As expected, values are higher that those shown for midlatitude stations in summer by *Groisman et al.* [1999]. Raising the threshold here to 0.1 mm lowers the GCM frequencies by typically 0.1 or 0.2, leaving them closer to these station values. The global mean π drops from around 0.80 to 0.68 as the threshold is raised, with much of the reduction being over polar regions as minimal 'drizzle' is excluded. The results for the threshold 0.1 mm, including global means over land and ocean, are then very similar to those presented by *Semenov and Bengtsson* [2002].

[16] In the warmer climate of 2071–2100, the overall wet day frequency is reduced slightly (Table 2). Zonal mean frequencies in the subtropics decrease, while near the equator and in the polar regions in summer frequencies tend to increase. The zonal means of the dry day frequencies $(1 - \pi)$ for January are depicted below.

[17] The distribution of daily precipitation amounts (up to 10 mm) in January at three particular grid squares (chosen from a sample set of 18, mostly representing inhabited land) is illustrated by histograms in Figure 7. In the two midlatitude land squares there is a clear peak at the 0 to 0.1 mm band, but there are also occurrences much larger than 10 mm. The tropical square (Figure 7b) has a much more centralized distribution.

[18] To display the latitudinal variation of rainfall amounts, values from each longitude have been combined and a contour graph of the resulting distributions constructed, as plotted for January in Figure 8a. Following *Hennessy et al.* [1997], a logarithmic amount (x) axis is used so that the full range can be seen easily. In order to preserve the net frequency at any latitude the frequency density function, f, is multiplied by the amount variable P. This leads to values tending to zero at small P. The greater intensity of equatorial rain and the frequent light precipitation (around 0.02 mm d^{-1}) near the winter pole are seen. A single peak occurs at nearly all latitudes.

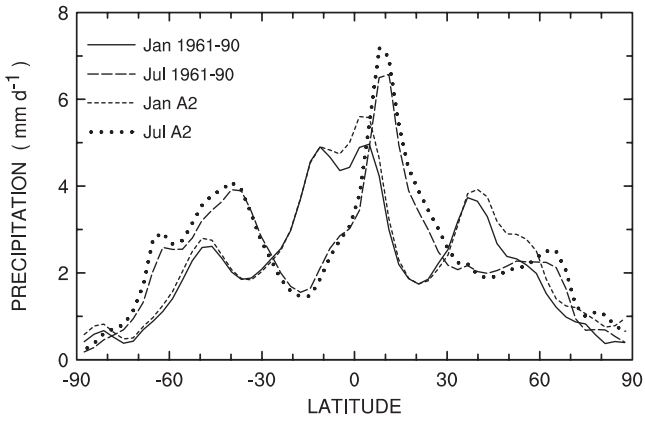

Figure 4. Zonal mean of precipitation rate simulated by the CSIRO GCM in January (Jan) and July (Jul) and two ensemble means. "1961–90" is the average over those years from the five extended simulations, while "A2" is the average over years 2071–2100 of the A2 ensemble.

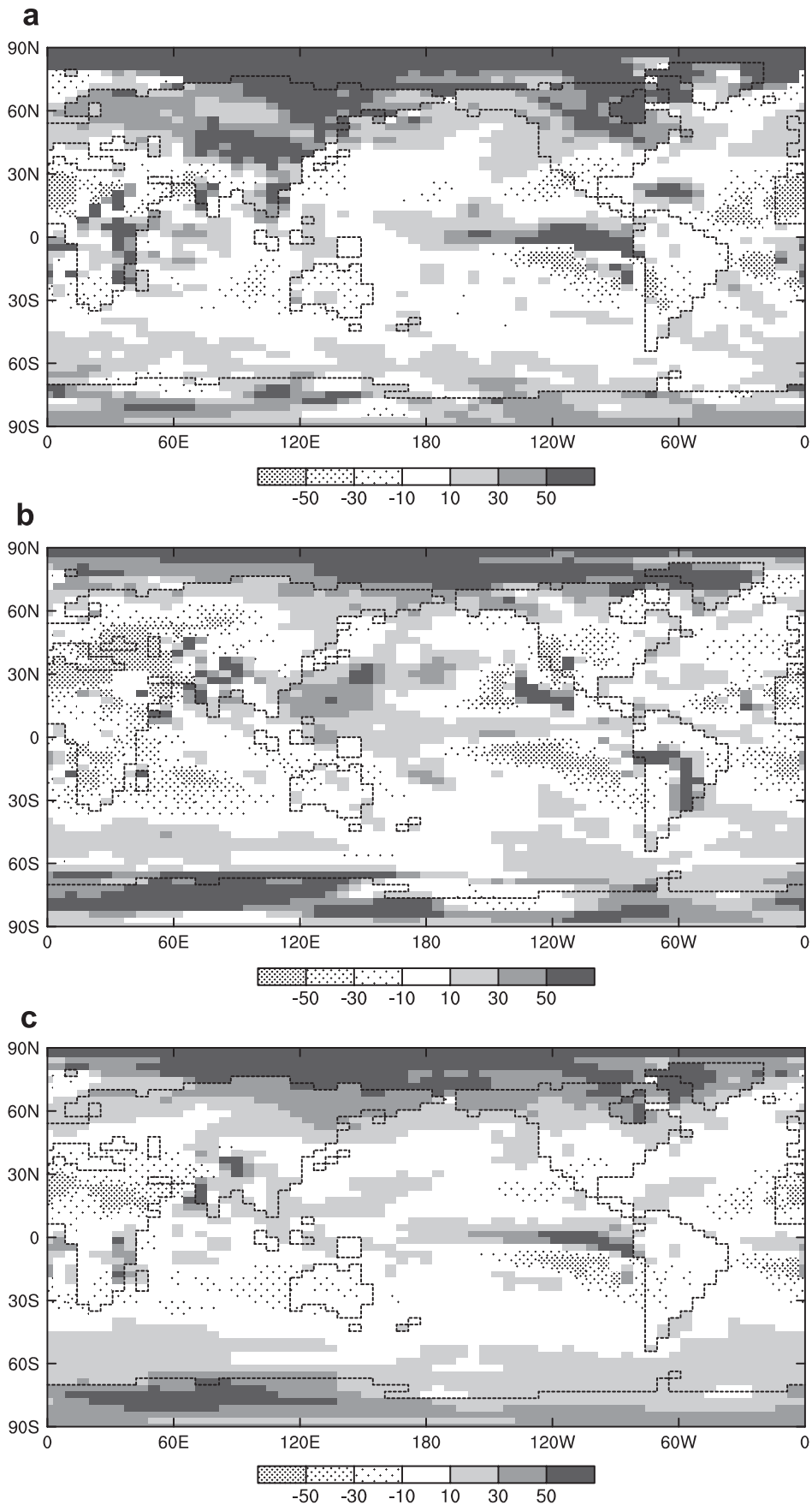

Figure 5. Percentage change in mean precipitation rate from 1961–1990 to 2071–2100, A2 scenario: (a) January, (b) July, and (c) annual.

Table 2. Global Means of Quantities in the Months January and July Determined for the Period 1961–1990, Together With Percentage Changes (of the Global Means) to 2071–2100, Under the A2 Scenario[a]

	1961–1990 Mean		Change, %	
Quantity	January	July	January	July
P	2.73 mm	2.82 mm	6.7	6.4
π	0.82	0.77	−2.4	−3.6
α	0.87	1.09	−2.0	−6.8
β	4.69 mm	3.86 mm	17.3	18.0

[a]P is the mean daily precipitation (including all days). π is the fraction of rain (wet) days (threshold, 0.0017 mm). α and β are the parameters of the gamma distribution fitted using moments to the rain day precipitation amounts values at each grid square (excluding those with 10 or fewer rain days in the 30 months of each period). Averages over the five simulations for each period are used.

[19] Changes in the January frequency distributions as a function of latitude are plotted in Figure 8b. At nearly all latitudes, even those where the dry day frequency increases, there is some shift in the distribution of wet day amounts toward heavier events (as evidenced by the banded structure).

3.2. Approximation by the Gamma Distribution

[20] Following previous authors, we use the gamma distribution as an approximation to the wet day frequency distributions. As detailed in Appendix B, the method of moments has been used to determine the shape, α, and scale, β, parameters. This has been applied at each grid square and month, run by run, with the parameters then averaged over the five ensemble members (as with other quantities). Note that values have not been defined where there are 10 or fewer rain days in any of the five 30-month samples (covering about 2% of the globe in each case). Global means of the two parameters for the 1961–1990 period are given for both January and July in Table 2. Examples of the gamma distributions are given in Figure 7. The gamma curves compare well to the histograms (as quantified in Appendix B), although there are discrepancies in some bands. Distribution curves for gamma parameters determined using the previously used method of maximum-likelihood (M-L) [*Thom*, 1958; *Semenov and Bengtsson*, 2002] are also shown. A third method, L-moments [*Hosking*, 1990], gives results (not shown) that are usually intermediate in character to the other two.

[21] Zonal means of the scale parameter in January from the three fitting methods are shown in Figure 9. The averaging over the 64 longitudes of the model grid allows clear differences between the methods to emerge from the grid square variations. The Figure 7c case typifies the midlatitudes, with greater extremes than for the curve determined by M-L, which gives smaller β than for the moment estimator. In contrast, for tropical distributions, as in Figure 7b, β is typically larger for M-L. The causes of these differences are considered in Appendix B. While the global means of each parameter of M-L are within 10% of those in Table 2, the spatial standard deviations of α are some 25% smaller for M-L than for moments, because of these latitudinal variations. As we will see, for much of the globe the skill of moment estimates in matching extremes is superior, and this, together with the ease of calculation and interpretation, leads us to focus on results from this method.

[22] Global maps of the parameters fitted by moments are shown for the January case in Figure 10. There are clear regional variations in both parameters, with β being largest in the subtropics, particularly over oceans. Zonal means of α, shown in Figure 11, peak near the equator. The relatively low equatorial values of β contrast with those found in some other studies, as will be discussed in section 5.

[23] The dominant change in the parameters ongoing to the 2071–2100 climate is an overall increase in β, given in Table 2. Local increases of 50% can occur, as seen in Figure 12. At many locations, however, particularly in the subtropics, β decreases. Zonal means of the changes are shown in Figure 13. While the global mean percentage changes approach those of the water column W, like P there is not a ubiquitous increase, and equatorial values barely change on average, unlike W (Figure 3). Changes in α are relatively small, but there are zonal mean decreases at most latitudes, as evident in Figure 11. This contrasts somewhat with the pattern of trends of α determined by *Semenov and*

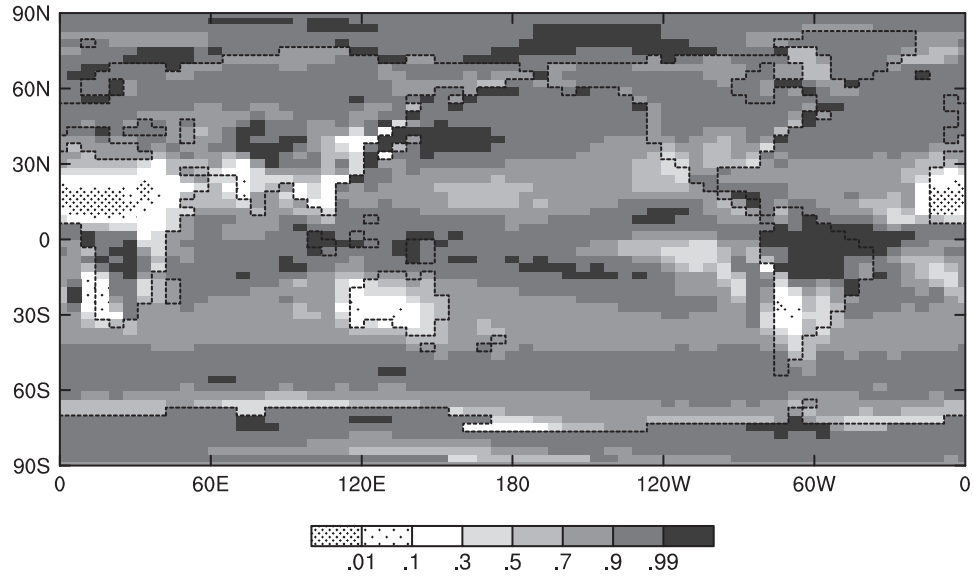

Figure 6. Fraction of wet days π for January, 1961–1990, with threshold 0.0017 mm.

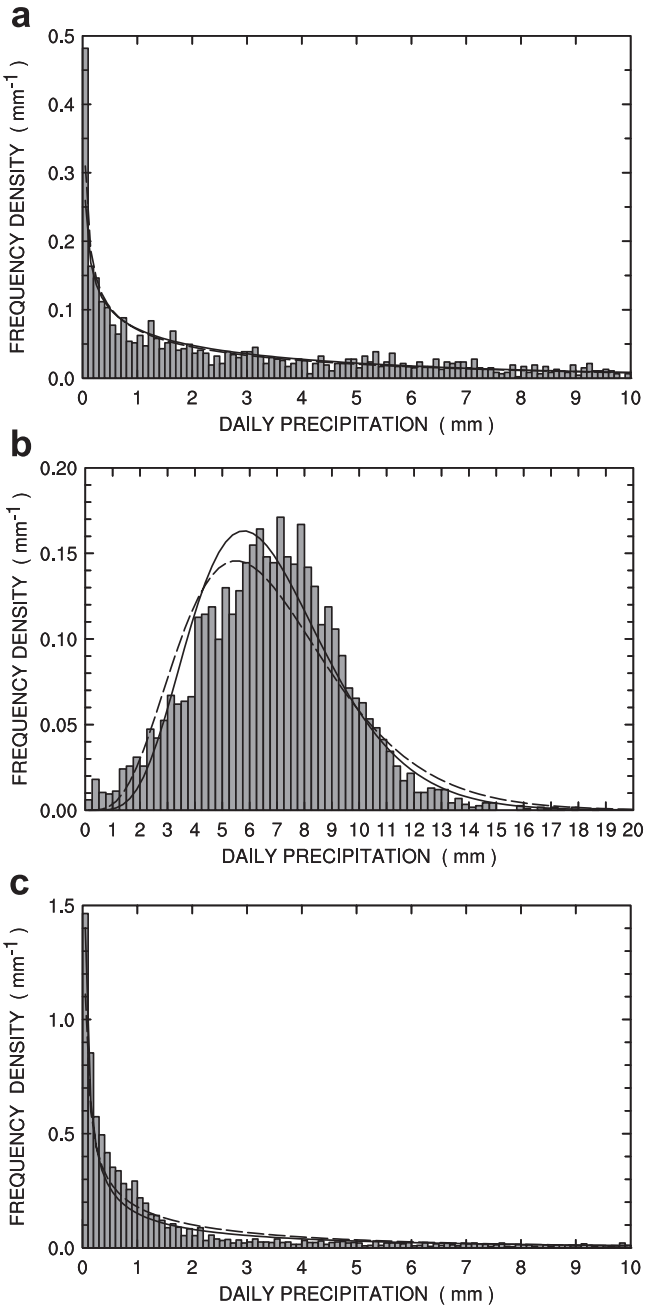

Figure 7. Frequency density of daily precipitation at each of three grid squares from all 4650 January days of 1961–1990, shown as a histogram, omitting the dry day frequency. The curves show the corresponding gamma distribution fitted using moments (solid) and by maximum likelihood (dashed), and scaled so that the net frequency (above the threshold) matches that of the histogram, i.e., π. The squares are (a) SE Australia, 37°S, 146°E, with $\pi = 0.40$, $\alpha = 0.62$, $\beta = 7.1$ mm (from moments), (b) Amazon, 5°S, 62°W, with $\pi = 1.0$, $\alpha = 6.8$, $\beta = 1.0$ mm, and (c) eastern United States, 37°N, 84°W, with $\pi = 0.88$, $\alpha = 0.29$, and $\beta = 8.2$ mm.

Bengtsson [2002], who find some substantial increases over subtropical oceans. Their trends in β include larger increases in the equatorial Pacific and more extensive decreases in the Southern Hemisphere.

3.3. Relation Between Means and Gamma Parameters

[24] The climatological monthly mean precipitation is simply related to the above gamma parameters (where defined) and the frequency by

$$P = \pi\alpha\beta, \tag{1}$$

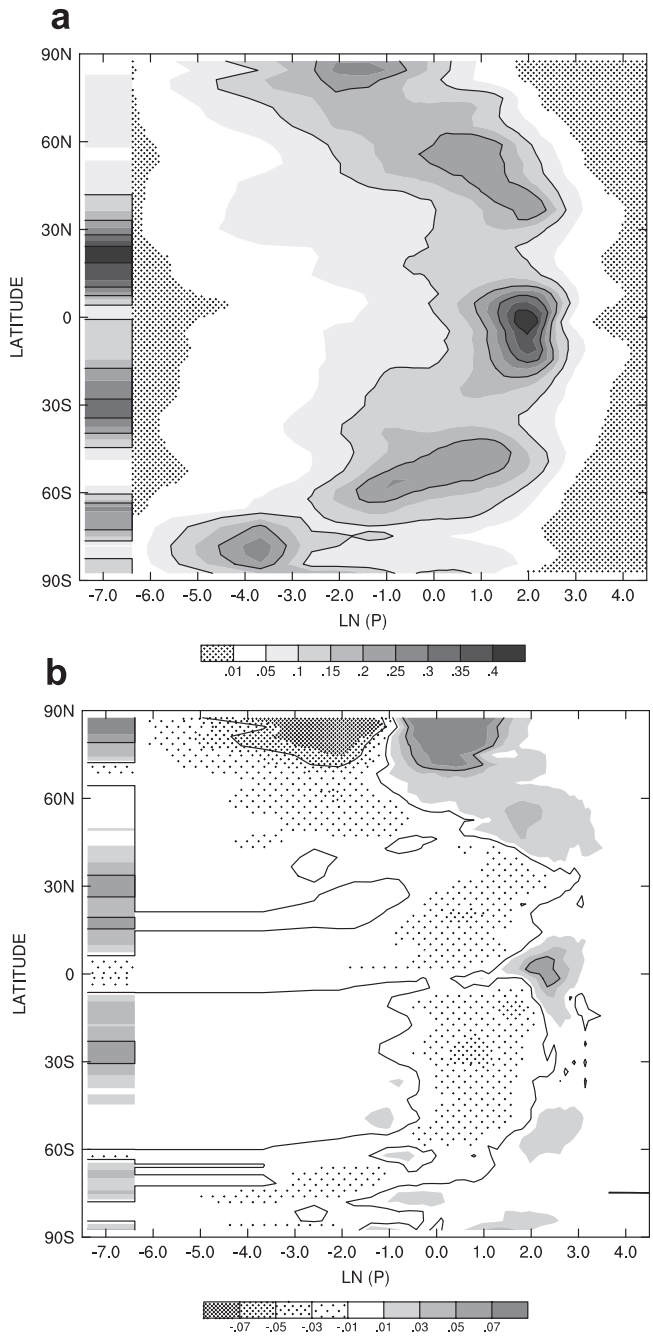

Figure 8. Frequency density (f) of daily precipitation (P), multiplied by the variable P (in mm), in January as a function of latitude for (a) 1961–1990 and (b) the change to 2071–2100, A2 scenario. A logarithmic x-axis is used. The fraction of dry days ($P \leq 0.0017$) is shown as a column of values without the P factor but with unit width, hence the total integral across the range at each latitude is one. The solid contour lines are: (a) 0.1, 0.2, 0.3, and 0.4; (b) −0.05, 0., and 0.5.

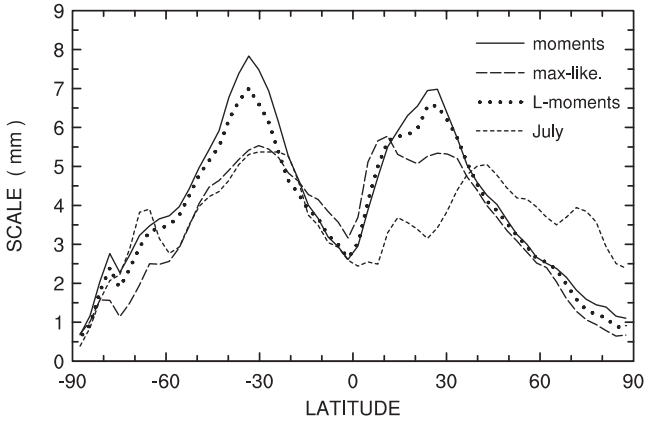

Figure 9. Zonal mean of the scale parameter (β) from each grid square, fitted to January rain day P values in 1961–1990. Three fitting methods are used: moments, maximum-likelihood, and L-moments. Also shown is the July result for moments.

(aside from a minimal difference, here, due to the ensemble averaging of parameters). We can therefore interpret the global spatial variation of monthly mean P in terms of these three component parameters. For the 1961–1990 climate and both January and July cases, the ratio of the spatial standard deviation relative to the mean is smallest for π and largest for α. The spatial correlation with P over the globe is also largest for α, around 0.6. However, the variations in P due to α are partly offset by those due to β, because of an anticorrelation between the two parameters with r around -0.3 in both months. While such an anticorrelation can result from having limited sample sizes (as noted by *Semenov and Bengtsson* [2002]), in this case it appears simply due to geographical variation. Relatively few locations have high values in both parameters, and hence very high rainfall rates. π is also well correlated with P, and weakly correlated with α.

[25] Linearizing the changes to equation (1) from 1961–1990 to 2071–2100, one has an additive relation between relative changes:

$$\Delta P/P \approx \Delta\pi/\pi + \Delta\alpha/\alpha + \Delta\beta/\beta. \qquad (2)$$

The sum of the three terms on the right do relate closely to the relative change in P, for each monthly case. The spatial correlations between the relative changes in P and those in the three components are given in Table 3. (Note that to avoid an unreasonable influence of locations where the denominator P is very small, a criterion is used.) The correlations indicate that all three quantities contribute to the pattern of changes in P. However, β appears to contribute least to the relative changes, despite its large average increase (Table 2).

4. Extremes of Daily Precipitation

4.1. Simulated Extremes of January and July Days

[26] We now turn to extremes of the daily precipitation data, partitioned by month, and compare the simulated values with those that can be anticipated from gamma distribution theory. For each month of the year the extreme (maximum) value has been calculated at each grid square, from each run and each period. Let us denote this the $E30$ statistic, being a 30-month (or year) extreme, from 930 days in the January and July cases featured here. Being a single-day value, at each square, these can vary considerably across the ensemble. Averaging the five results produces an estimate of the mean of the distribution of values that could be obtained with a larger ensemble. The field of averages for the 1961–1990 period are shown in Figure 14. Values reach 80 mm at some locations, but are typically around 30 mm at midlatitude land squares. Some of the small-scale spatial variation is due to the limited sampling. Global means of the average $E30$ are given in Table 4, along with those of $E150$, the maximum of the five values (hence a 150-month extreme, from a sample of one at each square). For both quantities the January mean is larger than the July mean, although the summer values are clearly larger in the high northern latitudes. Just as this seasonal contrast in the means does not match that of P (Table 2), neither does the $E30$ field closely relate to the P field. In this model, at least, there are relatively small extremes in the equatorial high-rainfall bands. The modeled extremes are clearly lower than observed station values over many parts of the globe, as discussed shortly.

[27] Percentage changes in the average $E30$ from 1961–1990 to 2071–2100 under the A2 scenario are shown in Figure 15. As a difference between means of (only) five cases, there is some noisiness evident in values between adjacent grid squares. Some subtropical regions exhibit consistent, small decreases. However, most changes are increases, some being substantial. The zonal means of the actual (non-relative) changes, shown in Figure 16, are all positive, except around 10°S in January. The global means increase around 14%, and a little larger for $E150$, as given in Table 4. The changes are thus substantially larger than for P (Table 2), although barely half those of W. Percentage increases in $E30$ are largest in the midlatitudes to high latitudes particularly in winter, with values over land typically 20 to 50%. There are substantial increases in $E30$ over much of the subtropical ocean, particularly in the Philippine Sea region, where mean rainfall also increases. However, as for the 1961–1990 case, there is only limited correspondence between mean and extreme changes globally. The spatial correlations for absolute or percentage changes are at most 0.6 (for absolute changes in July). A closer relationship holds between extremes and the scale parameter previously determined, as is evident from comparisons of the various figures. This prompts us to turn to the statistical theory for extremes.

4.2. Prediction of Extremes From the Gamma Distributions

[28] Following *Katz* [1999], let M_N denote the extreme value of P from N days. Assume, initially, that every day is wet and that P from each day is an independent random variable with a probability density function f with an asymptotically exponential tail, such as the gamma distribution. Then extreme value theory shows that the asymptotic distribution of M_N as N increases is the type I extreme value or Gumbel distribution with the cumulative distribution function

$$G(z) = \int_{-\infty}^{z} g(x)dx = \exp\left\{-e^{[-(z-u)/\lambda]}\right\}, \qquad (3)$$

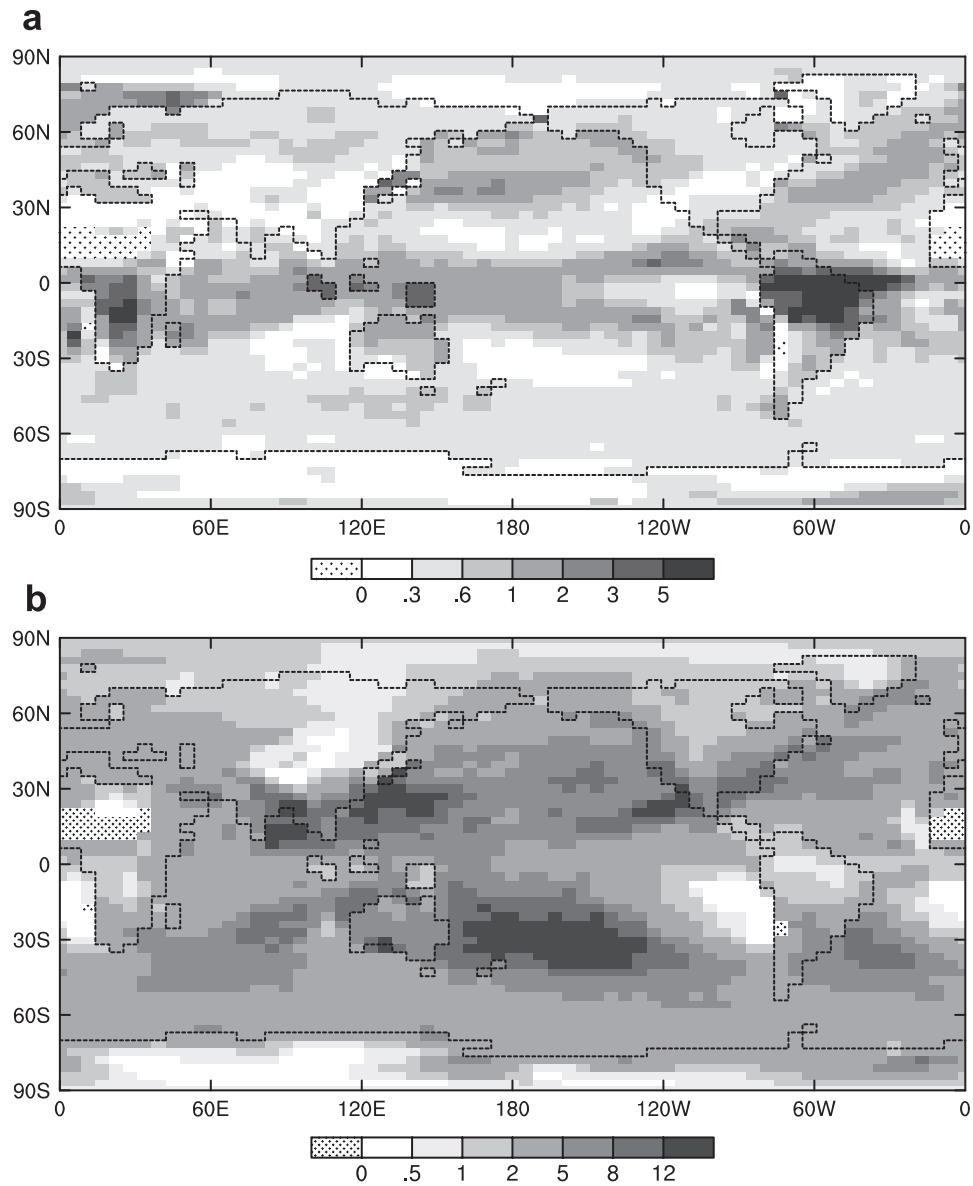

Figure 10. Gamma distribution parameters for January, 1961–1990: (a) shape parameter, α, and (b) scale parameter, β, in mm. Grid squares where no values are determined are dotted.

where the parameters u and λ are functions of N. The density function is

$$g(z) = \exp\left\{-e^{[-(z-u)/\lambda]} - (z-u)/\lambda\right)\Big\}/\lambda. \qquad (4)$$

For the gamma distribution with density function f and distribution function F, *Katz* [1999] notes that the asymptotic parameters (converted to the present form) are solutions of

$$1 - F(u) = 1/N \qquad \text{and} \qquad 1/\lambda = Nf(u). \qquad (5)$$

[29] If the succession of wet and dry days in a period is considered to be a stochastic process, the number of wet days would actually be a random variable with the expected value $N\pi$, using π as the unconditional probability of a wet day. *Katz* [1999] argues that for a Markov chain process the

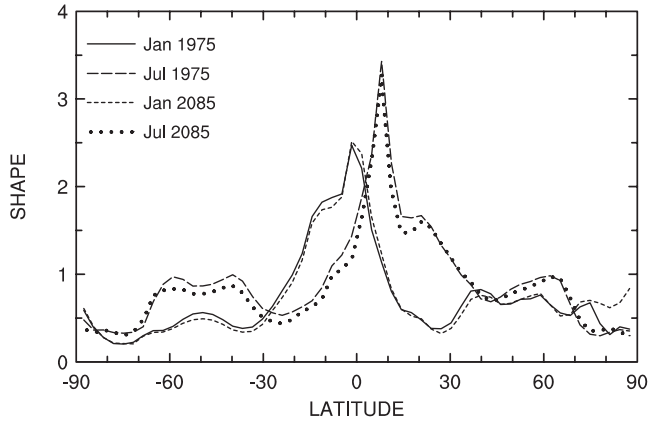

Figure 11. Zonal mean of shape parameter (α) for January and July and for periods 1961–1990, and 2071–2100, A2 scenario (marked by central year).

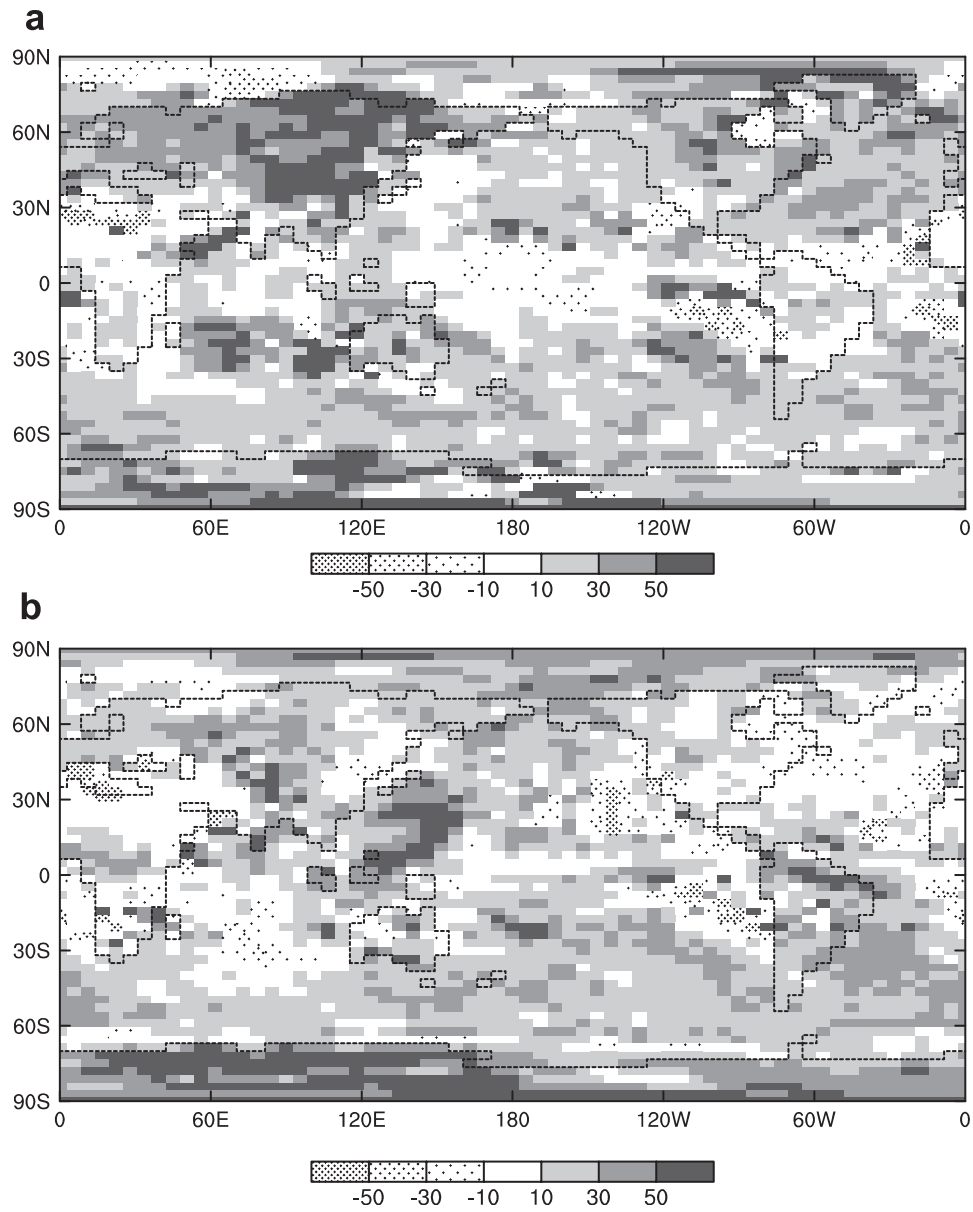

Figure 12. Percentage change in scale parameter (β) from 1961–1990 to 2071–2100, A2 scenario: (a) January and (b) July.

asymptotic result still applies if we simply replace N by $N\pi$ in equation (5). Given an algorithm for determining the inverse of F, the quantile distribution (see the Acknowledgments), the Gumbel parameters can be readily determined from equation (5), for any specification of the gamma parameters α and β, and $N\pi$. Experiments with randomly generated samples from gamma distributions indicate that the Gumbel distribution so determined closely matches the mean and variation of generated extremes across the parameter range of interest here. Following *Katz* [1999], we can also use the results for days taken from a single month, but over a number of years. For example, with $N = 930$ we determine a theoretical distribution of the $E30$ statistic for either January or July. It is worth noting that the parameters used by *Katz* [1999]

$$u = \beta(c + (\alpha - 1)\ln c) \qquad \text{and} \qquad \lambda = \beta, \tag{6}$$

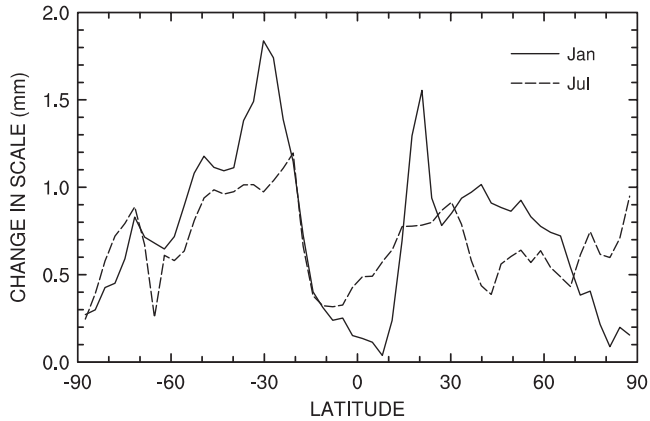

Figure 13. Zonal mean of the change in scale parameter in January (Jan) and July (Jul) from 1961–1990 to 2071–2100, A2 ensemble.

Table 3. Spatial Correlation r Between Percentage Change in P and Percentage Change in Other Quantities in the Months January and July[a]

	r	
Quantity	January	July
π	0.55	0.72
α	0.70	0.48
β	0.15	0.31

[a]Correlations are determined from grid squares where the 1961–1990 mean P is greater than 0.1 mm d^{-1}. The change is from 1961–1990 to 2071–2100, A2 scenario.

where $c = \ln [N\pi/\Gamma(\alpha)]$ are useful approximations to the solutions for $\alpha < 2$, but clearly fail for large α cases such as that in Figure 7b.

[30] As an example of this extreme value theory, Figure 17 shows a histogram representing the five GCM January $E30$ values for the southeast Australia grid square in 1961–1990, together with the Gumbel distributions for the 30- and 150-month extremes from the statistical model, based on gamma parameters fitted to the daily rain amounts. Consistent with the applicability of the theory, the five values are clustered around the median of the 30-month distribution (determined by solving $G(z) = 0.5$). Further, the average $E30$ value is approximated by the mean value of the relevant Gumbel distribution [e.g., *Zwiers and von Storch*, 1999, p. 49], given by

$$\mu = u + \gamma\lambda, \tag{7}$$

where γ is Euler's constant ($\approx$0.5772). For convenience, the means of the 30- and 150-month theoretical distributions are denoted $M30$ and $M150$. For cases where the theory holds, these estimates of the true means of the distribution of GCM

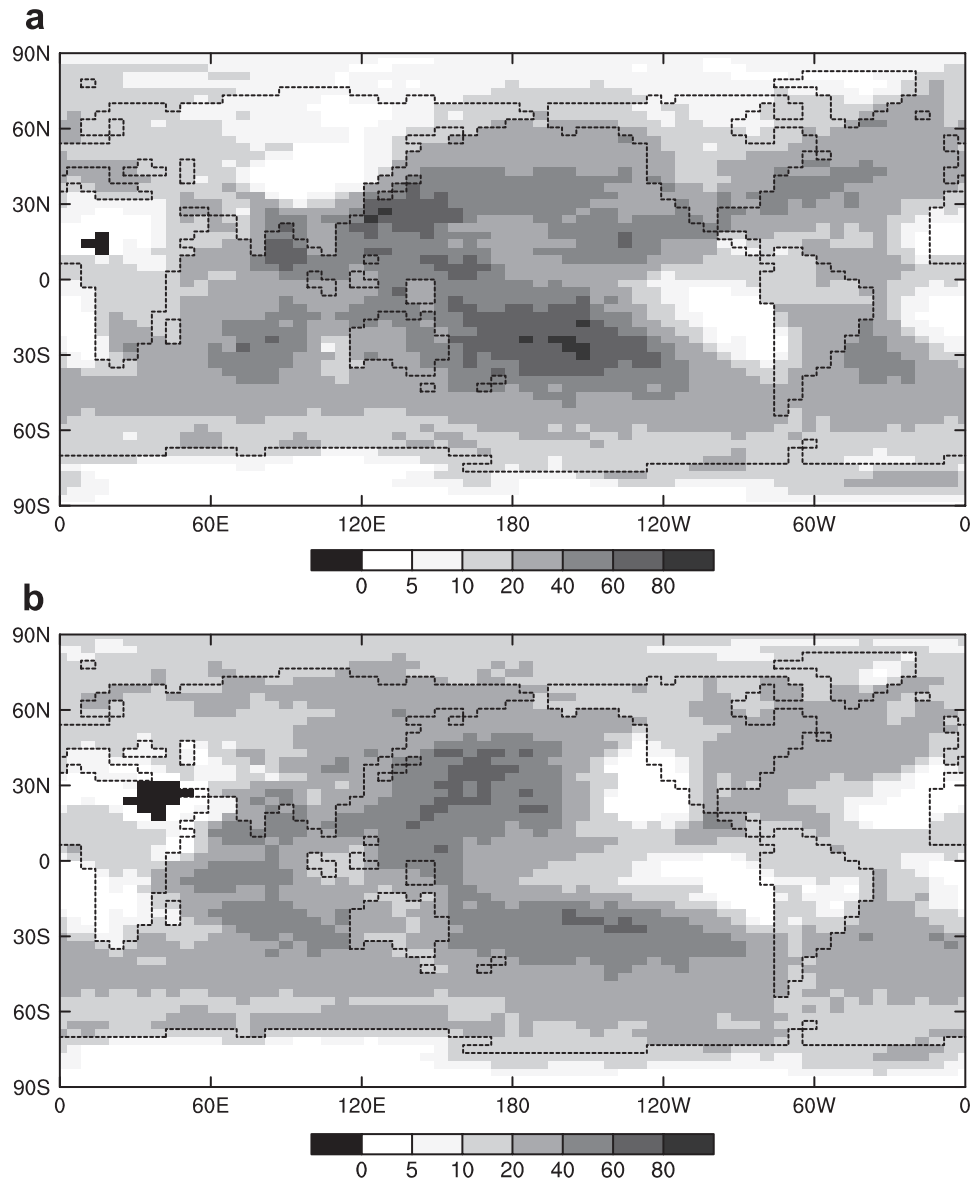

Figure 14. Extremes of daily precipitation, $E30$, during 1961–1990, during (a) thirty January months and (b) thirty July months. The means of values from the five runs of the ensemble are shown in each case. Squares with zero rain are shaded black.

Table 4. Global Means of Extremes of Daily Precipitation in the Months January and July Determined for the Period 1961–1990, Together With Percentage Changes (of the Global Means) to 2071–2100, Under the A2 Scenario[a]

	1961–1990 Mean, mm		Change, %	
Quantity	January	July	January	July
*E*30	27.9	24.2	13.6	13.8
*M*30	28.1	24.6	13.3	13.7
*E*150	35.3	30.5	14.9	15.1
*M*150	35.2	30.4	13.8	14.2

[a]*E*30 is the mean of values from five simulations (hence 30 months), and *E*150 is the extreme of values (hence 150 months). *M*30 and *M*150 are the corresponding results from Katz theory (equation (7), based on parameters determined using moments).

extremes should be useful, as they have relatively little sampling variability (that from the gamma parameters). Further, the Gumbel distribution can be used to give the likely range of extremes. The distribution can not be specified for grid squares where the gamma parameters were not defined. Since this occurs for cases with very few or no wet days it is reasonable to let *M*30 and *M*150 be zero then.

[31] Maps of *M*30 for the January and July cases are shown in Figure 18. In each case the correspondence with the average *E*30 field is very close, with spatial correlations of 0.97 for January and 0.96 for July. Even these correlations appear lowered by the sampling noise of *E*30: as anticipated the theoretical fields are spatially smoother. As a simple indication of the consistency of the theoretical distribution, squares with the median greater than or less

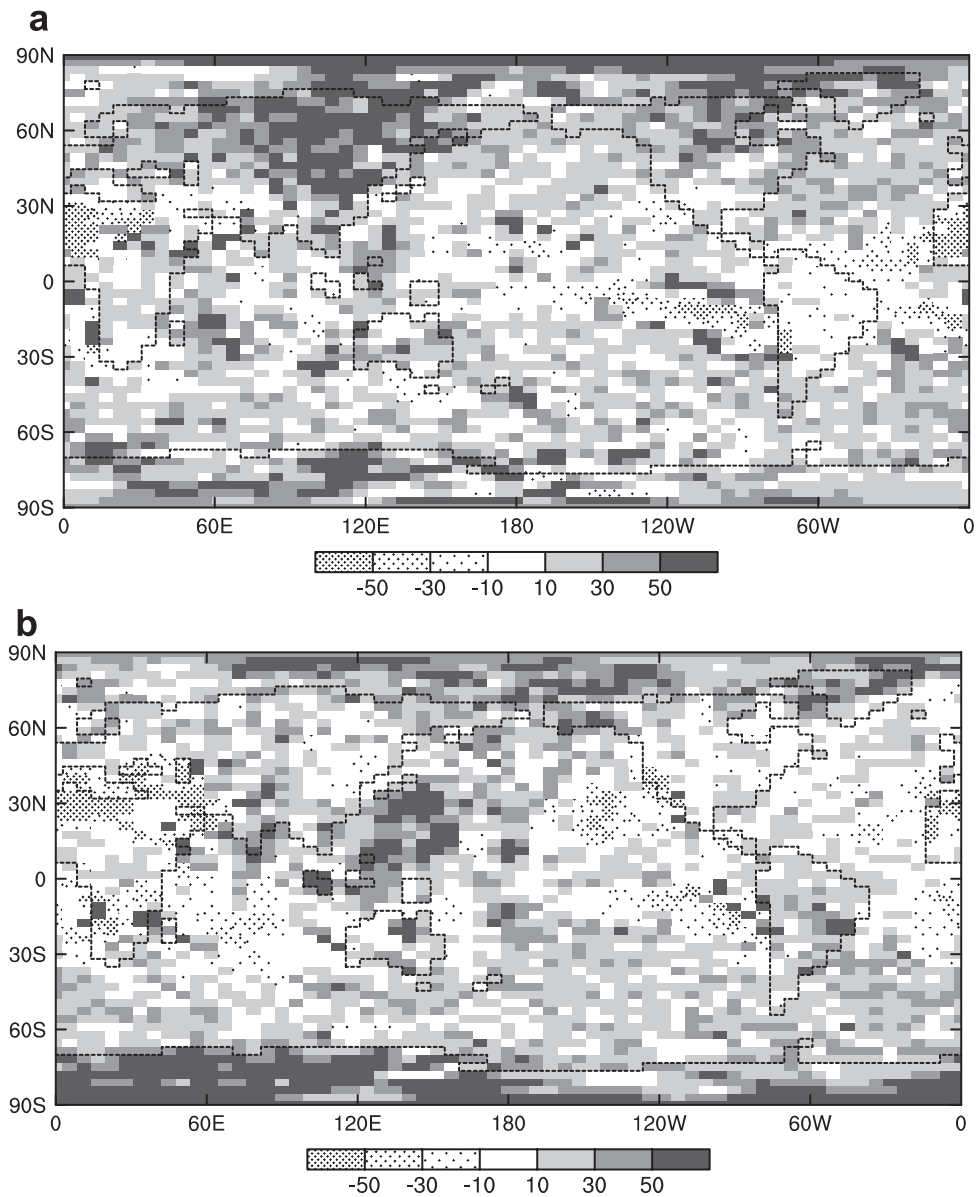

Figure 15. Percentage change in the extremes of daily precipitation, *E*30, from 1961–1990 to 2071–2100, A2 scenario, during (a) thirty January months and (b) thirty July months. Ensemble means are used.

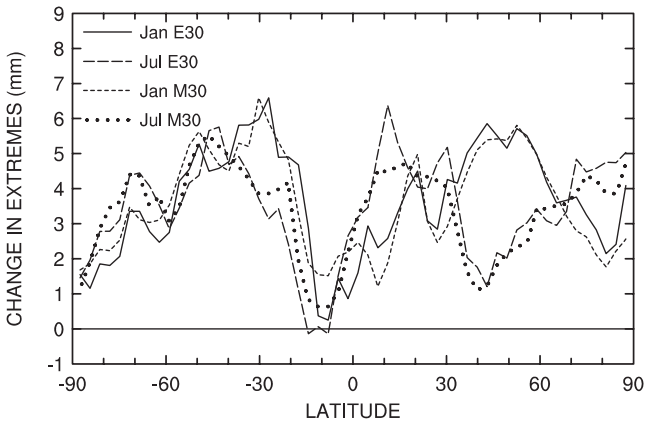

Figure 16. Zonal mean of the change in extremes of daily precipitation in January (Jan) and July (Jul), from 1961–1990 to 2071–2100, A2 scenario. Both simulated values, *E*30 (ensemble averages), and those from Katz theory, *M*30 (the expected values), are shown.

than all five *E*30 values are indicated in Figure 18. If the theory holds, one would expect each such event to occur by chance at 1 in 32 (2^5) squares, on average. The actual frequencies of the two events from squares across the globe are some two to five times this. For much of the globe, e.g., Australia, the theory seems valid, but there are regions where a consistent bias of *M*30 is evident, e.g., a positive bias in equatorial Africa and the United States in July, and a negative bias in some tropical oceanic regions. In zonal means, the *M*30 values are somewhat larger than the GCM extremes in the midlatitudes, by typically 5 to 10%, but are elsewhere usually quite close. Global means of *M*30 are similar to those of *E*30 (Table 4), suggesting that there is no overall bias in using the moment gamma distribution for extremes. However, values determined from the M-L fitted parameters match the global means less closely and the spatial correlations are below 0.87. In both months, over 60% of grid squares have an average *E*30 value that is closer to the moment *M*30, than the M-L or L-moment values.

[32] The *M*150 results from moment parameters are also a good match, in the global average, to the 150-month extremes, in each month (Table 4). Locally, sampling uncertainty in *E*150 can lead to considerable differences from the mean (or median) of the 150-month Gumbel distribution, as appears to be the case in Figure 17. Use of the gamma distribution theory for the prediction of extremes in additional simulations, or of return periods of extremes, would not be affected by this. Again, some regional biases are evident, with *M*150 being on average 10% too large in the midlatitudes.

[33] Turning to the changes in extremes due to global warming, we use the 2071–2100 gamma parameters to determine *M*30 and *M*150 for that period, and hence calculate the expected differences. The percentage change results for *M*30, shown in Figure 19, are again a good match to the GCM changes (aside from the noisiness of the latter), with spatial correlations between the fields of 0.75 (January) and 0.83 (July). The *M*150 percentage changes are very similar. The global means of the changes (Table 4) are also very close, as are the mean 30-year changes at each latitude (Figure 16).

[34] *Katz* [1999] noted that the theoretical extremes and return periods are particularly sensitive to variations in the scale parameter, and indeed the mean μ in equation (7) is linear in β, if other parameters are unchanged. For Mark 2, also, there are strong spatial correlations between β and *M*30, both for the 1961–1990 climate and the climate change fields, with *r* around 0.92 in each of the cases. Much of the latitudinal variation in the change in *E*30 (Figure 16) can thus be related to that of the change in β (Figure 13). The correlations show that the theory does improve over β alone as a predictor of relative changes in extremes, nevertheless, because changes in π and α also contribute.

4.3. Extremes From Any Month: Annual Case

[35] The extreme daily precipitation analysis has been applied to each of the twelve months of the year. Taking the maximum of the twelve monthly extremes for each simulation and each period provides an "annual" result that is the true 30-year extreme for each case. We then have a sample of five such values for each period. The average field of the 1961–1990 extremes is depicted in Figure 20a. The global mean of this annual result is 42.6 mm, considerably larger than any of the monthly values, which range from that in July (Table 4) to 28.0 mm for March. The global mean of the maximum of the five annual results (a 150-yr extreme) is 50.6 mm, reaching from 120 mm to 151 mm at several Pacific Ocean squares and a single land square ("North Japan"). The extreme over the United States is 86 mm in the southeast in October. The month and location relates well to observed U.S. extreme events averaged over areas comparable to the model grid squares by *Konrad* [2001]. The intensity falls somewhat short, although the comparison may not be fair, as noted previously.

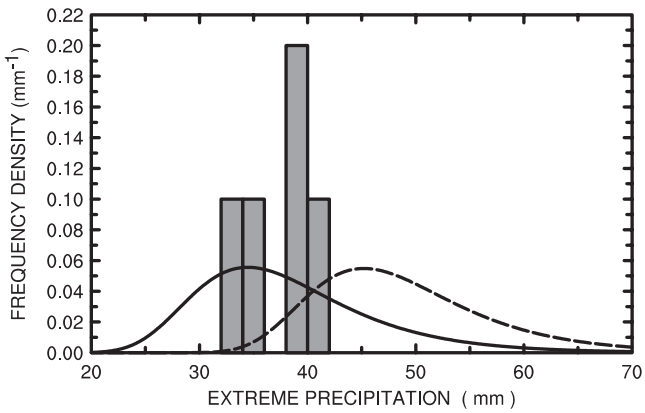

Figure 17. Frequency density of extreme daily precipitation at the SE Australia grid square from all (930) January days of 1961–1990, shown as a histogram of values from the five simulations, with bar width 2 mm. The curves show the Gumbel distributions determined from Katz's gamma model for both 30-month extremes (solid), and 150-month extremes (dashed). The 30-month median is 36.9 mm and *M*30 = 38.3 mm.

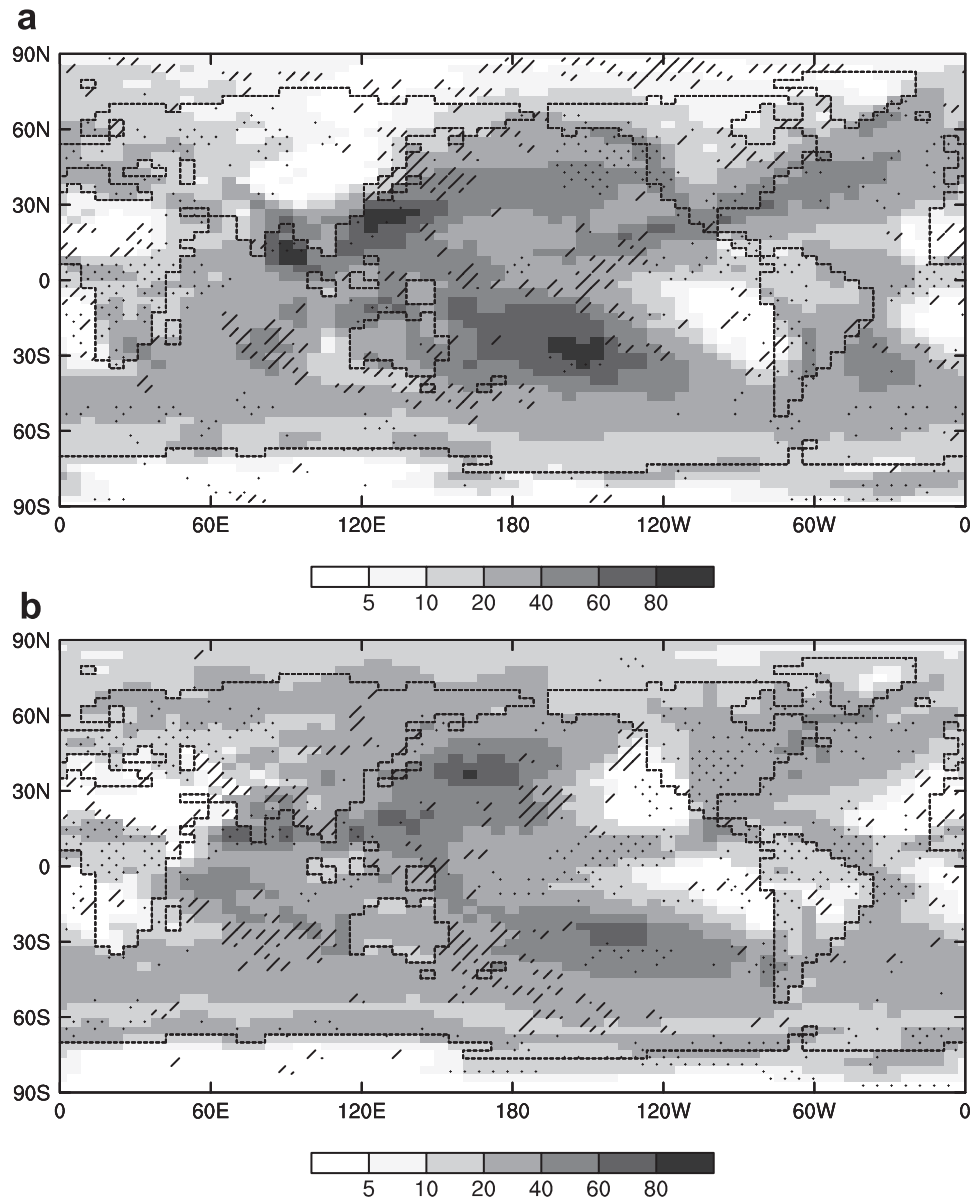

Figure 18. Mean value from Katz theory, $M30$, for extremes of daily precipitation during 1961–1990, during (a) thirty January months and (b) thirty July months. Squares where the theoretical median is greater (less) than all five $E30$ values are stippled (hatched).

[36] If there were no variation over the annual cycle in the daily rainfall distribution for a grid square, we might apply the Gumbel distribution theory directly to extremes from any month by simply letting N be the total number of days in the period (e.g., 30 × 365). However, for typical grid squares there is a substantial variation in the parameters of the Gumbel distribution, partitioned by month. Using the parameters averaged over the twelve months tends to underestimate the extremes.

[37] The standard development of extreme-value theory itself [e.g., *Zwiers and von Storch*, 1999, p. 49] provides a better approach for combining the monthly distributions. Let the extremes partitioned by month be E_i, for $i = 1, \ldots, 12$, and the extreme from any month be E_a. Then $E_a < z$ if and only if $E_i < z$ for each i. Thus, if the monthly variables can be considered independent, the cumulative distribution function for E_a is simply the product of the individual results:

$$F(z) = \exp\left\{ -\sum_{i=1}^{i=12} \exp[-(z - u_i)/\lambda_i] \right\}, \qquad (8)$$

where the parameters now have a subscript indicating the month. The corresponding density function can also be represented analytically and can be used to compute the distribution at each grid square, and hence the spatial fields of the means and medians for each period. In these calculations, months where the parameters are undefined because of having too few rain days can be simply omitted from the sums. Such months are unlikely to contribute to the GCM's 30-year extremes.

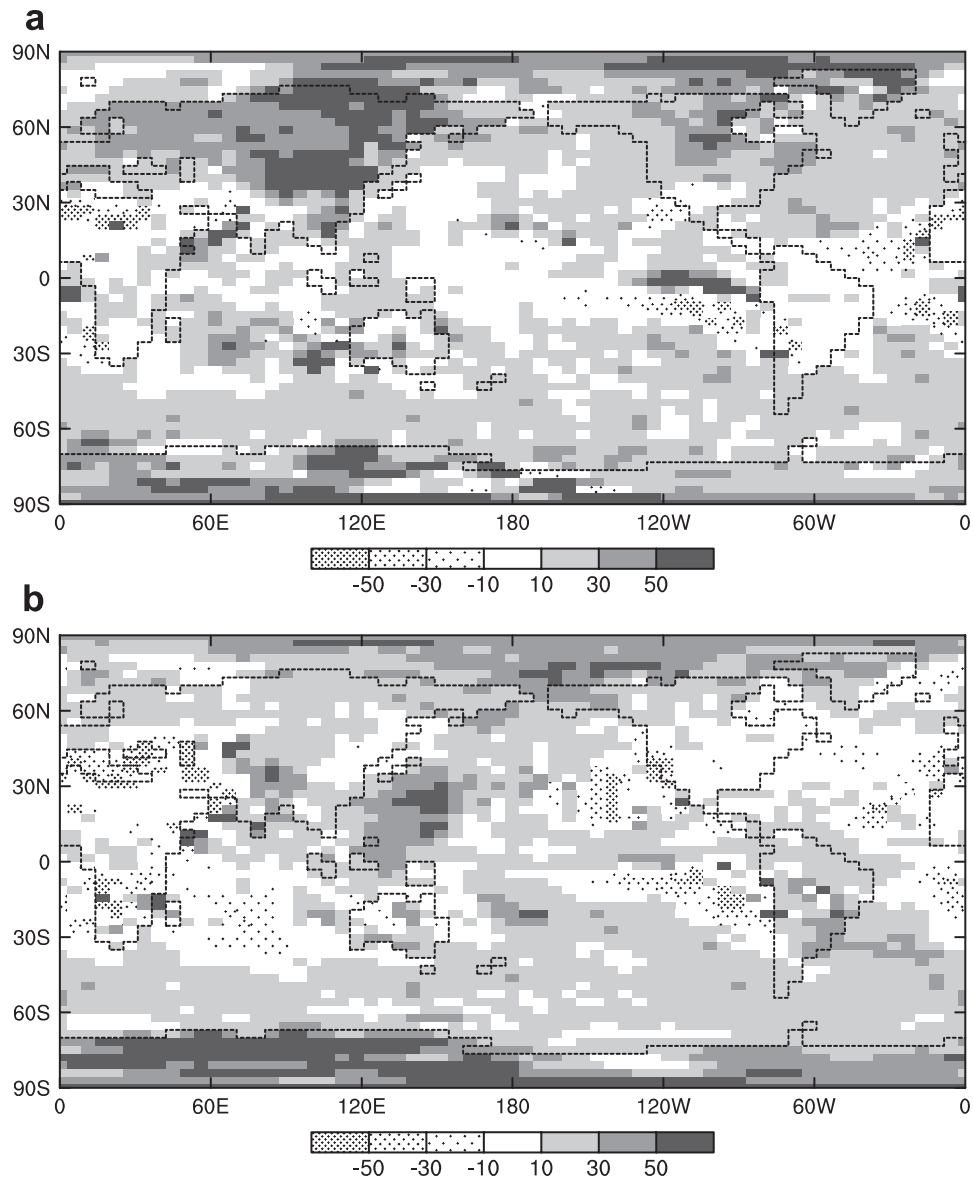

Figure 19. Percentage change in the mean value from Katz theory, *M*30, for extremes of daily precipitation from 1961–1990 to 2071–2100, A2 scenario, during (a) thirty January months and (b) thirty July months.

[38] The field for the expected value or mean of this theoretical 30-year extreme for 1961–1990 is depicted in Figure 20b. The agreement is very close over some regions, particularly given the sampling variability of the actual field. The shading indicates that the theory typically overestimates the GCM result for much of the midlatitudes, by on average 10% to 15%. In the tropics, the theory underestimates extremes by a similar amount over some of the ocean but overestimates them over Africa by 20% or more. Much of these biases relates to those in the individual monthly Gumbel distributions, in matching the *E*30 samples. The pattern of biases is similar to that of either the mean or the maximum of the twelve monthly results. In any case, the skill of the theoretical 30-year extremes is impressive, with the global mean only 3% larger than the GCM result, and a spatial correlation of 0.95. The bias in the mean is +5% for the 150-year extremes.

[39] The percentage changes from the GCM data in the 30-year extremes in 2071–2100 of A2, relative to 1961–1990, are shown in Figure 21a. Increases of 10 to 30% are common in the midlatitudes, in particular over Europe. Tropical changes are relatively small, except for increases in southern Asia, and some decreases, e.g., northern Africa. Increases of 30% or more are common in the high latitudes. The theoretical change field in Figure 21b shows similar patterns. It is much smoother than the GCM field, and for some purposes may provide a more reliable field than Figure 21a, over much of the globe. The change in the global mean of the theoretical 30-year extremes is 13.0%, close to the GCM result 13.8%. It should be acknowledged that for cases where the tail of the gamma distribution does not relate well to the extremes, such results may be less accurate than those determined from direct fitting of the extreme value distribution to a sample of larger daily precipitation values in

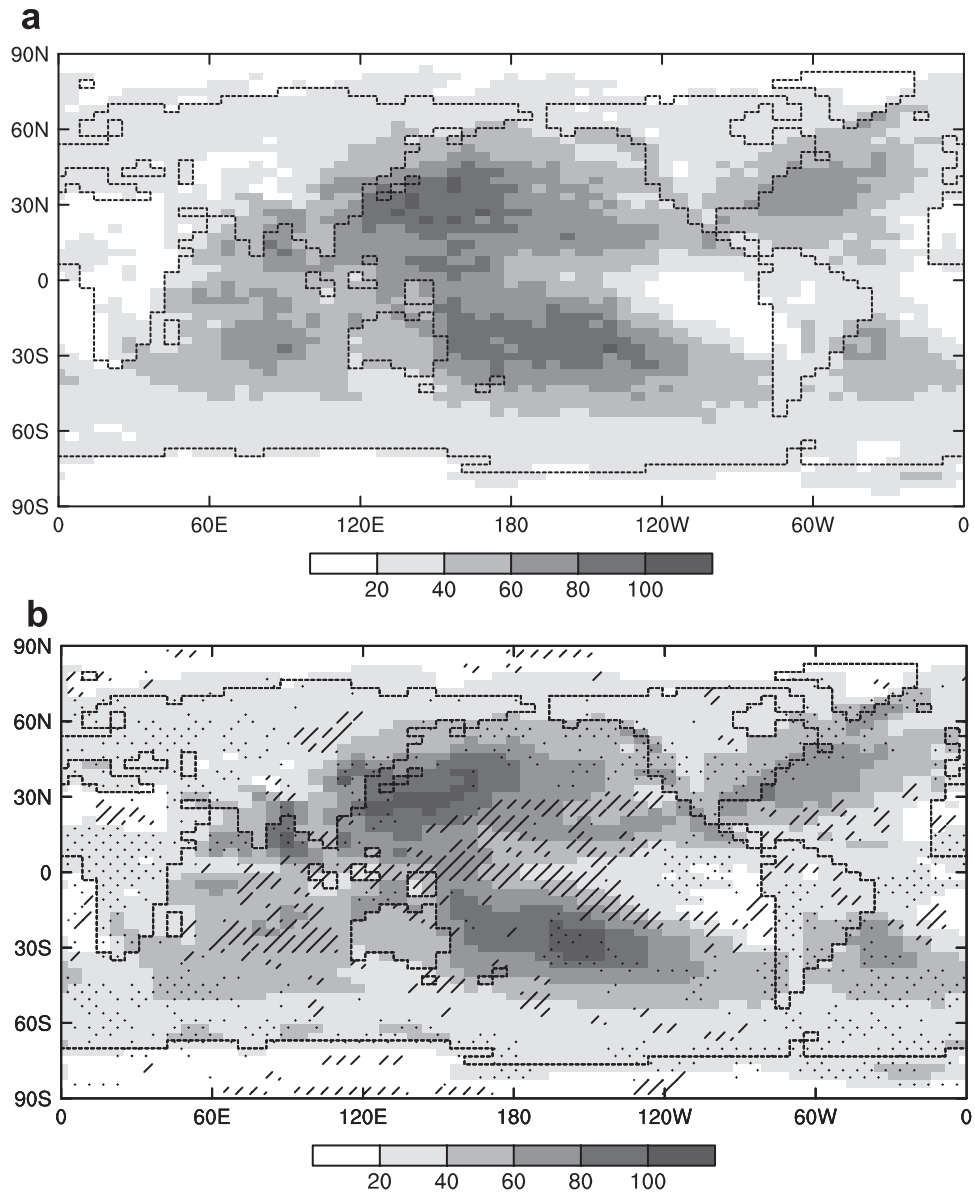

Figure 20. 30-year extremes of daily precipitation (the annual case) for 1961–1990 (a) ensemble means from the GCM and (b) the expected mean value determined theoretically by combining the Gumbel distributions for each month of the year, based on the gamma model. Squares where the theoretical median is greater (less) than all five GCM values are stippled (hatched).

each climate. For example, *Kharin and Zwiers* [2000] analyzed a sample of extremes from individual years. The present approach provides an interpretation of the extremes based on the monthly gamma distributions fitted to all days.

5. Discussion

[40] In this paper we have made use of the ensembles of transient climate simulations of the Mark 2 GCM to examine how the distribution of daily precipitation may change over the coming century. We have seen that the gamma distribution provides a useful representation of daily values in 30-year periods, even for extreme values, particularly for parameters determined by the method of moments. The increases in the scale parameter of the gamma distribution over midlatitudes and high latitudes seen in Mark 2 broadly coincide with those in the GCM assessed by *Semenov and Bengtsson* [2002]. The scale parameter changes relate closely to increases in the extremes, consistent with extreme value theory. Similarly, increases in 20-year return values of annual (single-year) extremes were derived from the CGCM2 simulations by *Kharin and Zwiers* [2000]. Less consistency between the three GCMs is evident at lower latitudes. Large increases in extremes in the subtropics occur in both Mark 2 and CGCM2. However, *Semenov and Bengtsson* [2002] find decreases in the scale parameter over much of the subtropical ocean. On the other hand, the changes near or at the equator in Mark 2 are relatively small, in contrast to some substantial increases in the other models. The Mark 2 behavior largely agrees with that of the earlier CSIRO models, described by *Gordon et al.* [1992] and *Hennessy et al.* [1997]. As they noted, the limited change near the equator is despite a large

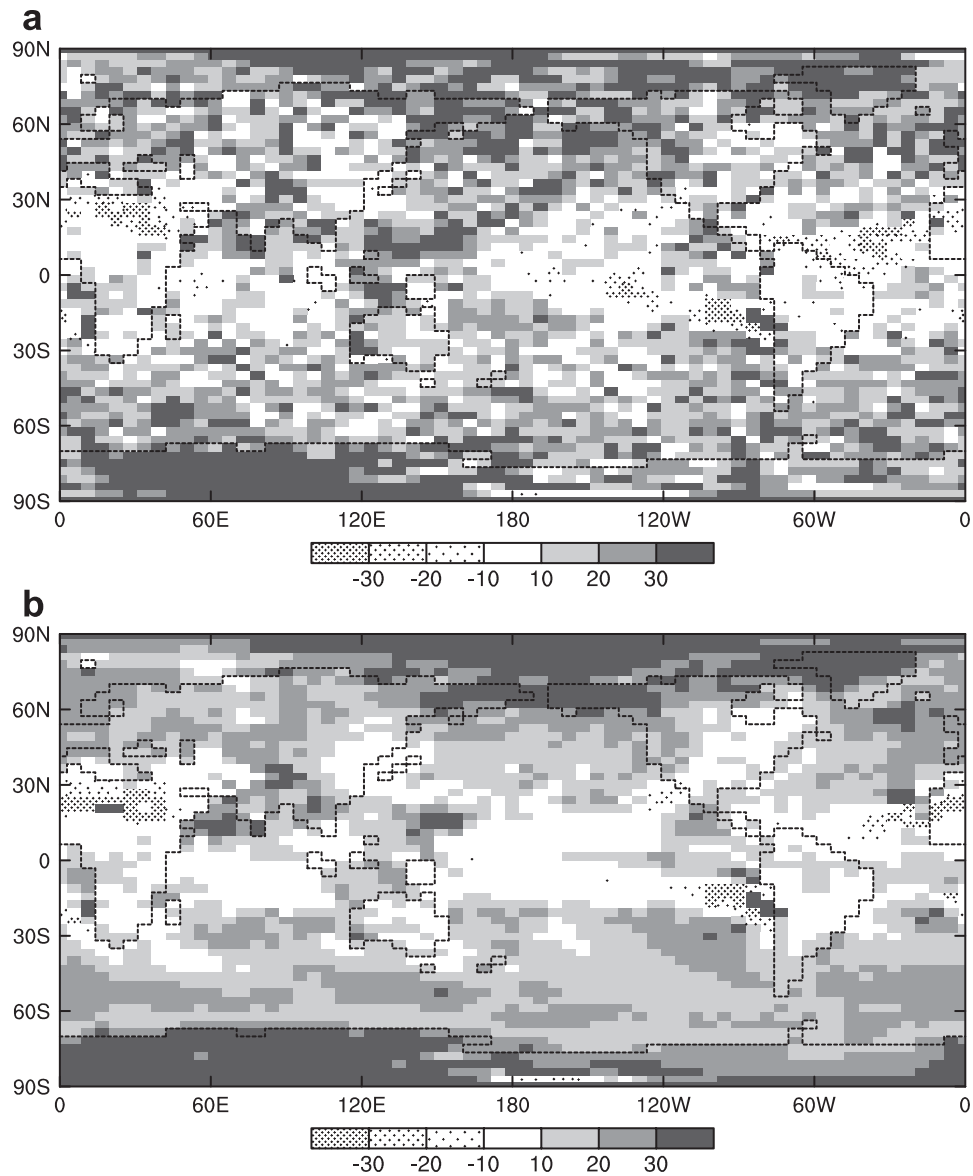

Figure 21. Percentage change in the 30-year extremes of daily precipitation from 1961–1990 to 2071–2100, A2, from (a) ensemble means from the GCM and (b) the theoretical expected values. Changes as large as ±50% occur at some places with small 1961–1990 values.

increase in humidity or W there. While it is reasonable to argue that increases in intensity tend to occur because of the greater water carrying capacity of the atmosphere in the warmer climate this does not apply everywhere.

[41] Equatorial differences between the CSIRO models and other GCMs also occur in the present climate daily rainfall distributions. Furthermore, 20-year return values evaluated from ECMWF reanalyses for 1979–1993 by *Kharin and Zwiers* [2000] also peak at the equator, in contrast to the Mark 2 extremes. Given that these rainfall data are determined from a GCM, and hence also represent grid square means, it is unclear how well these or the other GCM results relate to station or point rainfall. Presumably convection parameterizations, which determine nearly all the tropical grid square rainfall, at least in Mark 2, influence the daily rainfall distributions. Nevertheless, preliminary results from the GCM Mark 3, which has a different convection scheme (based on that used in the Hadley Centre's model), also show relatively low equatorial rainfall intensities, and scale parameter values. It is worth noting that the average β from Mark 3 is some 35% larger than for Mark 2, consistent with an increase anticipated from the increased resolution (the grid square areas being approximately 20% of those of Mark 2). Indeed, values averaged over the United States in July are 80% larger, comparable to the effects of such area averaging on observed extreme rain events [*Konrad*, 2001]. An extension of the approach of *Osborn and Hulme* [1998] to squares over the globe would be of great help in model validation.

6. Conclusions

[42] In a five-member ensemble of simulations of transient climate change by the CSIRO Mark 2 coupled GCM, including increased greenhouse gases and sulphate aerosol, the surface warming is close to the observed change over

1871–2000. Mean T then increases from 1961–1990 to 2071–2100 by 3.49 K under the A2 scenario, 29% more than for the B2 scenario, which has a very similar warming pattern then.

[43] The study focuses, initially, on the distribution of daily precipitation in the months January and July from 1961–1990. Much of the spatial variation of P is associated with the variation of wet day frequency, the remainder by the mean intensity of precipitation events, which tends to peak in the tropics. The gamma distribution provides a good approximation to such events at most locations in both months. In this GCM, the gamma's shape parameter is largest in the tropics, where low-rainfall days are infrequent, while the scale parameter peaks in the subtropics. Mean P increases some 6% by 2071–2100, under A2. Decreases occur in the subtropics, where they can be related to decreases in the frequency of dry days and also of moderate rain events, and hence the shape parameter. Over most regions the scale parameter increases, with the increase in the means being 18%.

[44] Consistent with extreme value theory, the scale parameter relates closely to the extremes of daily precipitation. The means over the five ensemble members of the 30-year extremes from January and July months of 1961–1990 are very similar to the theoretical results for the gamma distribution, both in the global mean and the spatial variation. The changes of these extremes in the later period are mostly increases, peaking in the subtropics. There are relatively small increases or even decreases around the equator in this model, consistent with the theoretical results based on the changes in the gamma parameters. Increases over the Northern Hemisphere land are typically larger in winter. The analysis is extended to the annual case, with increases again predominating. A theoretical result, obtained by combining the monthly distributions, provides good agreement, although positive biases of around 10% are common in the midlatitudes.

[45] The theory could be used to estimate return periods of extremes for this or other GCMs. The relative changes in gamma parameters could potentially be used for downscaling. Further use of the gamma distribution in interpreting variability of monthly precipitation can also be made, as will be described in a subsequent paper. Indeed, the different role of the gamma parameters in this variability, to that in the means, provides a basis for inferring information about extremes from these quantities.

Appendix A: Forcing and Initialization of the Transient Simulations

[46] The first Mark 2 ensemble completed was for the SRES A2 scenario of greenhouse gas (CO_2, CH_4, N_2O and CFCs) concentrations and SO_2 emissions [*Nakicenovic et al.*, 1998; *Cubasch et al.*, 2001]. The ensemble includes five simulations over the period 1991–2100. The radiative effects of the greenhouse gases were incorporated using a globally uniform equivalent-CO_2 concentration. The spatial distribution of atmospheric sulfate were determined using the NCAR Climate System Model following *Dai et al.* [2001]. The direct radiative effect of the sulfate was included as an adjustment to the surface albedo, based on *Kiehl and Briegleb* [1993]. Anticipated changes in the three-dimensional ozone distribution beyond 1990 from *Kiehl et al.* [1999] were also included.

[47] This initial ensemble was intended to represent uncertainty in future climate simply due to chaos originating in the atmosphere. The first member was a simple continuation of a simulation of the period 1871–1990 that incorporated estimated equivalent CO_2 and ozone changes together with the sulfate loadings based on the NCAR 1985 values, scaled by the annual emissions relative to that year. The 1871–1990 run, itself, followed a 150-year "control" simulation of the model using 1870 ozone concentrations and the base CO_2 concentration. Small perturbations in the model atmospheric or surface state at the end of 1990 were applied in the initialization of two further simulations over 1991–2100, and a fourth run was perturbed simply through round-off error associated with the use of a second computer. A fifth simulation was initialized by perturbing the initial run at the end of 1960.

[48] The spread of the global and annual mean surface temperature T from the (mostly) similar initial states in 1991 occurred within weeks, because of the rapid effect of chaos. There was little evidence of further spread in T in subsequent years, however, with the standard deviation (SD) of the five values at each year remaining typically less than 0.1 K.

[49] An enhancement in computer resources enabled the second "B2" ensemble to include five continuous simulations for the period 1871–2100. The first was the above 1871–1990 run, continued with the B2 CO_2 and sulfate scenario. Subsequent runs used the same suite of forcing, but were initiated at intervals of 50 years from an extension of the control simulation. This allowed the addition of uncertainty in the simulated future climate that might result from variation in the initial oceanic state.

[50] The initial years in B2 have some 20–30% more variation between the members than the initial years in A2, as might be expected. Later, though, the variations are similar, and the SD series from both ensembles seem largely consistent with the year-to-year internal variability of the control run. This internal variability of the coupled system is smaller than is observed [*Braganza et al.*, 2002], apparently because of the reduced amplitude of El Niño events in the model. In addition, other forcings of the climate system in the past century, in particular solar variations and volcanic disturbances, are missing from the GCM. In any case, the ensemble means of the annual mean values give a rather smooth mean warming series.

[51] It is evident that the form of initialization of the simulations does not lead to a major difference in climate variability between the runs, at least in the atmosphere. We will take each simulation as a plausible representation of the Earth's climate over the period simulated. The similarity of mean changes between the runs indicates that chaos, by itself, does not lead to a significant range of global warming in this model. The advantage of having five simulations in each case is to provide better sampling of the time periods, hence more certainty in the climate change signal. This is especially valuable for local results that are partitioned by the month of the annual cycle, and for daily extremes within each case.

Appendix B: Fitting the Gamma Distribution to the Wet Day Frequency Distribution

[52] The gamma distribution density function for daily amounts z is given by

$$f(z) = \left[(z/\beta)^{\alpha-1} e^{-z/\beta}\right] / [\beta\Gamma(\alpha)],$$

where α is the shape parameter, β is the scale parameter (in the units of z), and Γ denotes the gamma function. The method of moments [e.g., *Waggoner*, 1989] for determining the parameters, primarily used here, equates the mean P on wet days (the "precipitation intensity" P/π) to $\alpha\beta$ and the variance on such days to $\alpha\beta^2$. An alternative, the method of maximum-likelihood (which involves summation of the logarithm of sample values), is often favored as it can lead to greater efficiency in fitting the parameters of a true gamma distribution. Tests with randomly generated samples based on the cases in Figure 7 have shown that M-L values deviate from the original parameters by typically half as much as those from moments. The L-moment method has intermediate efficiency. However, with such large samples as in the present study such errors from moments are small and of limited concern. There is little mean bias in fitting using any of the methods.

[53] In practice, however, the GCM-simulated sample distributions are often not accurately gamma distributed, and this leads to significant differences between the results from the fitting methods, as noted in section 2. For example, in the Figure 7c case the M-L α is 53% larger, and the β 35% smaller, than the values from moments. The difference here appears to be due to a relatively flat distribution of values below 0.1 mm. The M-L curve, with its smaller α, is a better fit for this range. A similar difference between the methods is seen if a criterion is introduced into the true gamma experiments, even one as low as 0.0017 mm, which exceeds 9% of values in the moment-fitted curve, here. Fitting to values offset by the criterion, as done by *Semenov and Bengtsson* [2002], does not overcome the tendency for M-L to overestimate α, for cases when it is less than one, and the data do not adequately represent the gamma's asymptotic behavior. In contrast, the tropical case Figure 7b, indicates how some relatively small amounts can boost the M-L β. To compensate for the theoretical values less than the criterion, which are invalid, the curves in Figure 7 have actually been adjusted upward, preserving the rain day frequency. Likewise, the N values in equation (6) have been adjusted upward, producing a minor increase in $M30$.

[54] This sensitivity of the M-L method to the small values of daily precipitation may explain the larger midlatitude β values in this study than in some others that used M-L fitting. The better match of the extremes by moments in cases such as Figure 7c is a result of the larger β values. In addition, experiments where the large daily amounts in this case are progressively truncated indicate that M-L is also less sensitive than is moments to the extreme values. In any case, moments appear also slightly favored by the simple K-S statistic [*Kharin and Zwiers*, 2000] of the fit of a distribution (the peak error in the cumulative distribution function). Moments gave a better fit for 20 of the 29 cases with $P > 0.1$ from the sample set of 18 grid squares and two months noted previously. The average statistic of the 29 cases was 0.061 for moments and 0.074 for M-L.

[55] It is worth noting that the gamma fit to the data combined by latitude reproduces well the structure of both plots in Figure 8. The tendency of $f \times P$ toward zero at small amounts and the occurrence of a single peak are, indeed, properties of the gamma distribution. The area-weighted global mean K-S statistic for the 1961–1990 fit is 0.065 for January and 0.058 for July, similar to the mean for moments on the sample grid squares.

[56] **Acknowledgments.** This work contributes to the CSIRO Climate Change Research Program and is in part funded through Australia's National Greenhouse Research Program. The ACACIA consortium partially funded the initial GCM simulations. We thank Lawrence Buja of NCAR for providing the ozone and sulfate aerosol distributions used. The extension of the control simulation used in initiating the B2 ensemble was kindly provided by Siobhan O'Farrell. Comments from Steve Charles, Tim Harrold, Tom Beer, Richard Katz and the reviewers contributed to improvements in the presentation. Statistical software from J. Hosking's LMOMENTS package (available from http://lib.stat.cmu.edu/general/lmoments) has been used.

References

Boer, G. J., G. M. Flato, and D. Ramsden, A transient climate change simulation with greenhouse gas and aerosol forcing: Projected climate for the 21st century, *Clim. Dyn.*, *16*, 427–450, 2000.

Braganza, K., D. J. Karoly, A. C. Hirst, M. E. Mann, P. Stott, R. J. Stouffer, and S. F. B. Tett, Simple indices of global climate variability and change: Part I. Variability and correlation structure, *Clim. Dyn.*, *20*, 491–502, 2002.

Cubasch, U., G. A. Meehl, G. J. Boer, R. J. Stouffer, M. Dix, A. Noda, C. A. Senior, S. Raper, and K. S. Yap, Projections of future climate change, in *Climate Change 2001: The Scientific Basis*, edited by J. T. Houghton et al., pp. 525–582, Cambridge Univ. Press, New York, 2001.

Dai, A., T. M. L. Wigley, B. A. Boville, J. T. Kiehl, and L. E. Buja, Climates of the 20th and 21st centuries simulated by the NCAR Climate System Model, *J. Clim.*, *14*, 485–519, 2001.

Folland, C. K., et al., Observed climate variability and change, in *Climate Change 2001: The Scientific Basis*, edited by J. T. Houghton et al., pp. 99–181, Cambridge Univ. Press, New York, 2001.

Gordon, H. B., and S. P. O'Farrell, Transient climate change in the CSIRO coupled model with dynamic sea ice, *Mon. Weather Rev.*, *125*, 875–907, 1997.

Gordon, H. B., P. H. Whetton, A. B. Pittock, A. M. Fowler, and M. R. Haylock, Simulated changes in daily rainfall intensity due to the enhanced greenhouse effect: Implications for extreme rainfall events, *Clim. Dyn.*, *8*, 83–102, 1992.

Groisman, P. Y., et al., Changes in the probability of heavy precipitation: Important indicators of climatic change, *Clim. Change*, *42*, 243–283, 1999.

Hennessy, K. J., J. M. Gregory, and J. F. B. Mitchell, Changes in daily precipitation under enhanced greenhouse conditions, *Clim. Dyn.*, *13*, 667–680, 1997.

Hirst, A. C., The Southern Ocean response to global warming in the CSIRO coupled ocean-atmosphere model, *Environ. Model. Software*, *14*, 227–241, 1999.

Hosking, J. R. M., L-moments: Analysis and estimation of distributions using linear combinations of order statistics, *J. R. Stat. Soc., Ser. B*, *52*, 105–124, 1990.

Katz, R. W., Extreme value theory for precipitation: Sensitivity analysis for climate change, *Adv. Water Resour.*, *23*, 133–139, 1999.

Kharin, V. V., and F. W. Zwiers, Changes in the extremes in an ensemble of transient climate simulations with a coupled atmosphere-ocean GCM, *J. Clim.*, *13*, 3760–3788, 2000.

Kiehl, J. T., and B. P. Briegleb, The relative roles of sulfate aerosols and greenhouse gases in climate forcing, *Science*, *260*, 311–314, 1993.

Kiehl, J. T., T. J. Schneider, R. W. Portmann, and S. Solomon, Climate forcing due to tropospheric and stratospheric ozone, *J. Geophys. Res.*, *104*, 31,239–31,254, 1999.

Konrad, C. E., II, The most extreme precipitation events over the eastern United States from 1950–1996: Considerations of scale, *J. Hydrometeorol.*, *3*, 309–325, 2001.

Mearns, L. O., C. Rosenzweig, and R. Goldberg, Mean and variance changes in climate scenarios: Methods, agricultural applications, and measures of uncertainty, *Clim. Change*, *35*, 367–396, 1997.

Nakicenovic, N., N. Victor, and T. Morita, Emission scenarios database and review of scenarios, *Mitigation Adaptation Strategies Global Change*, *3*, 95–120, 1998.

Osborn, T. J., and M. Hulme, Evaluation of the European daily precipitation characteristics from the atmospheric model intercomparison project, *Int. J. Climatol.*, *18*, 505–522, 1998.

Roeckner, E., L. Bengtsson, J. Feichner, J. Lelieveld, and H. Rodhe, Transient climate change simulations with a coupled atmosphere-ocean GCM including the tropospheric sulfur cycle, *J. Clim.*, *12*, 3004–3032, 1999.

Semenov, V. A., and L. Bengtsson, Secular trends in daily precipitation characteristics: Greenhouse gas simulation with a coupled AOGCM, *Clim. Dyn.*, *19*, 123–140, 2002.

Thom, H. C. S., A note on the gamma distribution, *Mon. Weather Rev.*, *86*, 117–121, 1958.

Waggoner, P. E., Anticipating the frequency distribution of precipitation if climate change alters its mean, *Agric. For. Meteorol.*, *47*, 321–337, 1989.

Watterson, I. G., An analysis of the global water cycle of present and doubled CO_2 climates simulated by the CSIRO general circulation model, *J. Geophys. Res.*, *103*, 23,113–23,129, 1998.

Watterson, I. G., Interpretation of simulated global warming using a simple model, *J. Clim.*, *13*, 202–215, 2000.

Wilby, R. L., and T. M. L. Wigley, Future changes in the distribution of daily precipitation totals across North America, *Geophys. Res. Lett.*, *29*(7), 1135, doi:10.1029/2001GL013048, 2002.

Zwiers, F. W., and H. von Storch, *Statistical Analysis in Climate Research*, 484 pp., Cambridge Univ. Press, New York, 1999.

M. R. Dix and I. G. Watterson, Division of Atmospheric Research, Commonwealth Scientific and Industrial Research Organisation, PMB 1, Aspendale, Victoria 3195, Australia. (ian.watterson@csiro.au)